Global trends in carbon sinks and their relationships with CO_2 and temperature

Authors: M. Fernández-Martínez[*1]. J. Sardans[2,3,] F. Chevallier[4], P. Ciais[4], M. Obersteiner[5], S. Vicca[1], J. G. Canadell[6], A. Bastos[4], P. Friedlingstein[7], S. Sitch[7], S.L. Piao[8,9], I.A. Janssens[1], J. Peñuelas[2,3].

Affiliations:

[1] Centre of Excellence PLECO (Plant and Vegetation Ecology), Department of Biology, University of Antwerp, 2610 Wilrijk, Belgium.

[2] CSIC, Global Ecology Unit, CREAF-CSIC-UAB, Cerdanyola del Vallès, 08193 Barcelona, Catalonia, Spain

[3] CREAF, Cerdanyola del Vallès, 08193 Barcelona, Catalonia, Spain

[4] Laboratoire des Sciences du Climat et de l'Environnement, CEA CNRS UVSQ, 91191 Gif-sur-Yvette, France

[5] International Institute for Applied Systems Analysis, Schlossplatz 1, 2361 Laxenburg, Austria

[6] Global Carbon Project, CSIRO Oceans and Atmosphere, Canberra, ACT 2601, Australia

[7] College of Engineering, Computing and Mathematics, University of Exeter, Exeter EX4 4QF, UK

[8]Sino-French Institute of Earth System Sciences, College of Urban and Environmental Sciences, Peking University, Beijing 100871, China

[9] Institute of Tibetan Plateau Research, Chinese Academy of Sciences, Beijing 100085, China

*Correspondence to: M. Fernández-Martínez, marcos.fernandez-martinez@uantwerpen.be

Elevated CO_2 increases photosynthesis and, potentially, net ecosystem production (NEP) meaning greater CO_2 uptake. Climate, nutrients, and ecosystem structure, however, influence the effect of increasing CO_2. Here, we analysed global NEP from MACC-II and Jena CarboScope atmospheric-inversions and 10 dynamic global vegetation models (TRENDY), using statistical models to attribute the trends in NEP to its potential drivers: CO_2, climatic variables and land-use change. We find that increasing CO_2 was consistently associated with increased NEP (1995-2014). Conversely, increasing temperatures were negatively associated with NEP. Using the two atmospheric inversions and TRENDY, the estimated global sensitivities for CO_2 were 6.0 ± 0.1, 8.1 ± 0.3 and 3.1 ± 0.1 Pg C per 100 ppm (~1 ºC increase), and -0.5 ± 0.2, -0.9 ± 0.4 and -1.1 ± 0.1 Pg C $°C^{-1}$ for temperature. These results indicate a positive CO_2 effect on terrestrial C sinks that is constrained by climate warming.

In recent decades, terrestrial ecosystems have been absorbing 15–30% of all anthropogenic CO_2 emissions[1,2]. Direct and indirect anthropogenic impacts on the biosphere, however, can alter terrestrial sinks in the short and long terms[3–6]. Identifying the factors that affect the capacity of the biosphere to absorb carbon (C) and quantifying the magnitude of the sensitivity of this C sink to its driving factors helps to increase confidence in future projections of the coupled C cycle/climate system.

Increasing plant growth is a robust response to increasing CO_2 concentrations under experimental conditions (CO_2 fertilization effect)[7,8]. The extent to which increases in CO_2 can enhance large-scale photosynthesis and ultimately net ecosystem production (NEP) remains uncertain[5,7]. Detecting this effect in the real world is much more difficult than under controlled experiments. However, recent efforts using eddy-covariance-based data and statistical models have been successful in detecting positive effects of CO_2 on water-use efficiency (WUE)[9], photosynthesis, and NEP[5].

The potential positive effect of elevated CO_2 on productivity could be influenced by global warming[6] and altered precipitation patterns[10] since both water availability and temperature are strong drivers of photosynthesis and respiration worldwide[11–13]. Land-use change also alters the capacity of the biosphere to sequester C because land use causes a drastic change in C turnover and productivity. Atmospheric deposition of nitrogen (N) and sulphur (S) from the use of fossil fuels and fertilisers may also alter ecosystem biodiversity, function, productivity and NEP[5,14–17]. N deposition is usually positively correlated with ecosystem productivity and NEP[17–19]. Conversely, S deposition may reduce ecosystem carbon sinks, this has rarely been investigated in field studies[20,21] and absent from global models. Soil acidification, caused by acid deposition, of N and S, often decreases the availability of soil nutrients[22] and potentially reduces NEP[23].

The observations underlying the driver analysis of NEP described above were largely limited to temperate and boreal study sites, making it difficult to assess global scalability. Additionally, until recently, the only way to assess terrestrial C sink was from ensembles of dynamic global vegetation models (DGVMs) or as a residual sink, by subtracting atmospheric and ocean sinks to the estimates of CO_2 emissions. Currently, inversion models, as well as long-term remotely sensed data[24], can be used to test the generality of the patterns derived from ground-based measurements. Inversion models provide continuous gridded estimates for the net flux of land-atmosphere CO_2 exchange (i.e. NEP) with global coverage[25,26]. The gridded NEP results from inversions, combined with CO_2-concentration records, gridded fields for climate, land-use change, and atmospheric deposition, are arguably the best observation-based data to attempt a first empirical study of the combined effects of CO_2, changes in climate and land use, and atmospheric N and S deposition on terrestrial NEP patterns at the global scale. Given that previous site level studies revealed that increasing CO_2 is a dominant driver of trends in NEP, we expect that it will also be the dominant driver at larger spatial scales and across the globe.

Here we investigate if the trends of NEP from the two most widely used multi-decadal inversion models (MACC-II and Jena CarboScope) and DGVMs (TRENDY) from 1995 to 2014 are related to increasing atmospheric CO_2 and changing climate (temperature, precipitation, and drought). Additionally, the effect of land-use on NEP at the global scale was investigated using statistical models to assess the sensitivity of NEP to the abovementioned predictors. We also analysed the effect of changing rates of atmospheric deposition of oxidised and reduced N and S on NEP, combined with increasing CO_2 and changing climate and land use, over Europe and the USA.

CO_2 and climate effects on global NEP

Global land (excluding Antarctica) mean annual NEP was 2.3 ± 0.9, 2.3 ± 1.5 and 1.6 ± 0.5 Pg C y^{-1} (mean ± 1σ), respectively, for MACC-II, Jena CarboScope and the TRENDY ensemble during the period 1995–2014, similar in magnitude to the recent global carbon budget[2]. Both inversions and the TRENDY ensemble showed an overall positive trend in NEP from 1995 to 2014. The estimated NEP increased by (mean ± 1SE) 116.9 ± 6.1 Tg C y^{-1} for the MACC-II dataset, by 178.0 ± 8.1 Tg C y^{-1} for the Jena CarboScope dataset, and by 22.5 ± 3.1 Tg C y^{-1} for the TRENDY ensemble (**Figure 1**). This supports the increases in the global carbon budget[2], with a lower increase of the DGVMs than those shown by the inversion models. The large differences between inversion models and DGVMs may arise because of the lack of information on river fluxes, inadequate parameterisations concerning land management and degradation in the process models or because of potential biases in inversion models. Both inversion model datasets produced similar trends for many parts of the world, an increasing NEP for Siberia, Asia, Oceania, and South America, and a decreasing NEP for the southern latitudes of Africa. Differences between inversions emerged for Europe and North America, possibly because Jena CarboScope inversion uses a larger spatial error correlation of prior fluxes than MACC-II or because of other inversion settings[2]. However, their different flux priors did not drive differences in the trends between both datasets, given that priors did not change over the studied period. Jena CarboScope showed largely positive trends for Europe and largely negative trends for North

America; MACC II showed more variation in the trends for both continents. The trends identified by the TRENDY ensemble agreed with atmospheric inversions for the northernmost latitudes, indicating an increase in C-sink capacity, but differed from those in many other regions.

Our analyses on temporal contributions, using the temporal anomalies of our predictors, attributed the increases in global NEP to increasing CO_2 but found a consistent negative impact of temperature on NEP, which limited the positive effect of increasing CO_2 (**Figure 1**). These results were consistent for both datasets and most of the DGVMs of the TRENDY ensemble. The predictors used in this study explained a modest proportion of the variance in NEP, in contrast to the variance explained by spatial variability (i.e., the pixel), which was rather high (**Supplementary Information (SI), Section 2**). Unknown contributions to trends in NEP, the difference between all contributions and the observed trend, were very close to zero for the analyses on inverse models and the TRENDY ensemble (**Figure 1**). This result suggests that trends were very well captured by our analyses, indicating that the methodology was able to disentangle spatial from temporal variability. The sensitivity of NEP to increasing CO_2 averaged 0.45 ± 0.01, 0.61 ± 0.03 and 0.23 ± 0.01 g C m^{-2} ppm^{-1} for MACC-II, Jena CarboScope and TRENDY, respectively **(Table 1)**, representing sensitivities over the entire terrestrial surface of 60.4 ± 1.2, 81.4 ± 3.4 and 30.7 ± 1.2 Tg C ppm^{-1}, respectively. Despite lower temporal attributions for temperature than CO_2, the sensitivity of NEP to temperature was high, at -3.8 ± 1.1, -6.4 ± 2.9 and -8.1 ± 0.9 g C m^{-2} y^{-1} $°C^{-1}$ for the MACC-II, Jena CarboScope and TRENDY models, respectively, equivalent to global sensitivities of -515.7 ± 152.4, -859.2 ± 386.3 and -1088.0 ± 118.1 Tg C $°C^{-1}$, respectively. Trends in NEP and the effect of CO_2 and temperature on NEP significantly differed in magnitude amongst the datasets used, however, they all point towards the same conclusion: global NEP has increased during the study period and increasing CO_2 has been the most likely driving factor despite increasing temperatures constraining this positive effect. The exact magnitude of the effect of increasing CO_2 and temperatures on global carbon cycle remains to be established

Spatial variability on CO_2 and climate change effects on NEP

Our statistical models for the MACC-II and Jena CarboScope datasets indicated that the positive effect of CO_2 on NEP was higher in regions with higher annual precipitation and that this positive effect increased with increasing temperatures (**Figure 2, SI Section 1.1**). In contrast, our analyses using the TRENDY ensemble did not show a significant interaction between CO_2 and precipitation or with temperature, highlighting the different behaviour in the DGVMs compared to inversion models. We also found a significant positive interaction between mean annual temperature and CO_2 for Jena CarboScope and TRENDY. However, the same interaction was negative for MACC-II. On the other hand, increasing temperatures reduced NEP in warm regions but increased NEP in cold regions (**Figure 2**).

The analyses on temporal contributions performed for inversion and TRENDY NEP averaged over latitudinal bands (boreal, >55°; temperate, 35-55°; subtropical, 15-35°; and tropical, 15°N-15°S), further supported previous results obtained at the global scale (**Table 2, SI Sections 2.2–2.7**). Increasing CO_2 was the main factor accounting for increasing trends in NEP, with a consistent positive temporal contribution for almost all latitudinal bands considered and for all three datasets. However, contributions estimated from the TRENDY ensemble were generally lower than those of the inversion models. Proportionally, increasing CO_2 accounted for more than 90% of the trends in NEP in MACC-II and Jena CarboScope datasets. For the TRENDY ensemble, the estimated contribution of CO_2 to the trends in global NEP was more than 2.7 times higher than the estimated trends. Increasing temperatures had a negative effect for all latitudinal bands for the inversion models, but most effects were not statistically significant and need to be interpreted as such. Instead, our analyses for the TRENDY ensemble indicated a significant negative effect for all latitudinal bands, except for the temperate southern hemisphere. Similarly, the proportional contribution of temperature to the trends in NEP was less than 10% for the inversion models, but accounted for almost 95% of the trends estimated using the TRENDY ensemble. These results suggest that the parameterisation of temperature in the DGVMs does not accurately reproduce the estimation of the inverse models.

Despite all regions presented, on average, positive trends, the tropical regions clearly had the highest contribution, across all three datasets, to global NEP trends accounting for almost half of the increase (**Table 2**). Similarly, the tropical regions had the highest sensitivity to CO_2 increase, accounting for more than half of the total global sensitivity (**Table 1**). A similar pattern was found for temperature, although the sign of the contribution was positive for MACC-II but negative for Jena CarboScope and TRENDY. The contribution of the southern hemisphere to the global trends was very modest compared to the contribution of the northern hemisphere using all datasets. Our results using the MACC-II dataset showed that subtropical, temperate and boreal regions of the northern hemisphere accounted for 44.2% of the global trends in NEP, while only 9.5% was attributed to subtropical and temperate regions of the southern hemisphere. Using the Jena CarboScope dataset these regions accounted for 63.3% and 6.1%, respectively. Differences on the regional attributions between inversion models may emerge from the different interhemispheric transport models or other inversion settings[2]. Results from the TRENDY ensemble were more extreme, because they indicated a negative contribution of the subtropical and temperate regions to the global trends in NEP. Differences between the global estimates (trends and contributions of CO_2 and temperature) and the sum of every region were low for all datasets. Contribution of other variables to the trends in NEP (precipitation, drought, land-use change, and unknown variables) were on average also low for most of the latitudinal bands, despite the variability amongst datasets (**Table 2**).

Atmospheric deposition

The MACC-II and Jena CarboScope datasets showed that NEP increased over Europe and the USA by 0.45 ± 0.13 and 0.68 ± 0.16 g C m^{-2} y^{-1}, respectively (**Figure S1**). Our temporal contribution analyses suggested that increasing atmospheric CO_2 in both datasets contributed significantly to increasing NEP. NEP sensitivity to CO_2 was more than two-fold higher in the Jena CarboScope than the MACC-II dataset (**Table S1**), similar to the temporal contributions, at 0.22 ± 0.06 and 0.46 ± 0.07 g C m^{-2} y^{-1} ppm^{-1} for the MACC-II and Jena CarboScope models, respectively. The temporal contribution of decreasing N_{OX} deposition to NEP differed between the two datasets; the contribution was positive for MACC-II and negative for Jena CarboScope. Our analyses consequently estimated a negative sensitivity of NEP to N_{OX} for the MACC-II dataset but a positive sensitivity for the Jena CarboScope dataset. Additionally, neither MACC-II, nor Jena CarboScope indicated a strong impact of land use change.

These statistical models indicated that, in both datasets, the positive effect of CO_2 on NEP was higher in regions with higher N_{RED} deposition but lower in regions with high S deposition (means for MACC-II and annual anomalies for Jena CarboScope; see **SI section 2.8**). The results for N_{OX} deposition, however, differed between the models. The positive effect of CO_2 on NEP for the MACC-II dataset was constrained by the annual anomalies of N_{OX} but was higher for the Jena CarboScope dataset. We also estimated an overall negative but not significant sensitivity of NEP to S deposition for both inversion models.

CO_2 fertilisation and global NEP

The positive effect of atmospheric CO_2 on NEP must originate from a stronger positive effect on photosynthesis than on the sum of all respiratory processes. Increasing atmospheric CO_2 concentrations have been widely reported to increase ecosystem photosynthesis, mainly by two mechanisms: i) increasing carboxylation rates and decreasing photorespiration[27], and ii) decreasing stomatal conductance and therefore increasing WUE[9,28], which would theoretically increase photosynthesis under water limitation. An increase in GPP by either mechanism may thus account for the higher NEP due to increasing atmospheric CO_2. A recent global analysis suggested that most of the GPP gains from CO_2 fertilization are associated with ecosystem WUE[29]. The positive interaction between CO_2 and annual precipitation that we found may not support this hypothesis (**Figure 2**), given that plants living under wet conditions are usually less efficient in water use. However, plants having higher water availability may benefit from increasing CO_2 more than those suffering drought because photosynthesis would not be water-limited.

Our estimates of global NEP sensitivity to CO_2 were 0.45 ± 0.01, 0.61 ± 0.03 and 0.23 ± 0.01 g C m^{-2} ppm^{-1} (globally 60.4 ± 1.2, 81.4 ± 3.4 and 30.7 ± 3.4 Tg C ppm^{-1}) for the MACC-II, Jena CarboScope and TRENDY datasets, respectively, but these estimates varied amongst the latitudinal bands and were inconsistent between datasets (**Table 1**). These estimates were similar to those reported in CO_2-enrichment FACE experiments[30], despite the fact that FACE values were calculated for a much higher CO_2 range for which the effect of CO_2 may saturate[31]. However, they were much lower than the 4.81 ± 0.52 g C m^{-2} ppm^{-1} reported in a study using eddy-covariance flux towers for a similar period[5]. The much larger areas analysed by the inverse models than the footprints covered by the eddy-covariance flux towers, and FACE experiments, may explain these differences between the estimates. Flux towers are usually located in relatively homogenous, undisturbed ecosystems, while each pixel in the inverse model aggregates information from several ecosystems (and even biomes), often including non-productive land such as bare soil or cities.

Our results indicated that the variability of the estimates of NEP sensitivity to CO_2 amongst the latitudinal bands might be associated with differences in climate and atmospheric N and S deposition. The two atmospheric inversion models indicated that the effect of CO_2 fertilisation was stronger in wet climates (high annual precipitation) (**Figure 2**), supporting the estimates provided by the latitudinal bands, with the highest sensitivity estimates for the tropical band (**Table 1**). However, analyses based on the TRENDY ensemble did not show the same results. The positive effect of CO_2 tended to increase with temperature anomalies in both inversion models, but, again, the DGVMs did not show the same behaviour. These differences between inversion models and process-based models suggest that DGVMs still fail to capture some of the interactions occurring in nature. The MACC-II and Jena CarboScope datasets further agreed on a stronger positive effect of increasing CO_2 in regions with higher N_{RED} deposition, which confirms previous studies suggesting that the effect of CO_2 fertilisation is stronger in nitrogen-rich sites[32–34].

Climate, land-use and C sinks

Climatic warming clearly had a secondary effect on the trends in NEP from 1995 to 2014. The MACC-II, Jena CarboScope and TRENDY datasets estimated that NEP decreased globally by around -0.5 ± 0.2, -0.9 ± 0.4 and -1.1 ± 0.1 Pg C for every degree of increase in the Earth's temperature. Assuming that a CO_2 increase of 100 ppm is equivalent to an increase of global temperature of 1 ºC, the effect of the increasing CO_2 concentrations largely outweighs the negative effect of increasing temperature on NEP (global estimates: 6.0 ± 0.1, 8.1 ± 0.3 and 3.1 ± 0.1 Pg C for a 100 ppm of CO_2 increase according to MACC-II, Jena CarboScope and TRENDY). The difference, though, is much lower for TRENDY than for the inversion models, having a higher negative impact of temperature and a lower positive effect of CO_2. This difference in the effects of temperature and CO_2 may explain the lower trends observed in TRENDY datasets compared to MACC-II and Jena CarboScope. It also suggests that a different parameterisation of temperature, CO_2 and their interaction may be needed on DGVMs to capture the observed trends in the inversion models.

The quasi monotonically increasing atmospheric CO_2 concentrations have been more important than temperature in driving NEP trends. Increasing temperature, however, did not have the same effect on NEP around the world. The analyses of both inverse models indicated that increasing temperatures had a positive effect on NEP only in cold regions (when MAT ≤ 1.5, 9 and -5.9 ºC for MACC-II and Jena CarboScope and TRENDY respectively, when CO_2 = 400 ppm, see **SI section 2.1**, and **Figure 2**). These findings support previous literature reporting a positive effect between temperature increase and NEP in temperate and boreal forests[35]. Instead, the general negative effect of temperature on NEP could be due to a greater stimulation of Re than photosynthesis by higher temperatures[36,37]. The potential benefit to C sequestration of increased photosynthesis would then be negated by a greater increase in Re. Increasing temperatures can also be linked to heat waves and drier conditions, which may decrease GPP more than Re[38].

The effects of land-use change on NEP trends differed greatly amongst the datasets, both at the global scale and when using latitudinal bands. Our statistical models identified several significant relationships between NEP and land-use change, but the large differences in effects (direction and magnitude) amongst the datasets preclude drawing firm conclusions. The coarse resolution of analysis likely blurred the effects of land-use change on the NEP trends.

Our study highlights the dominant role of rising atmospheric CO_2 concentrations triggering an increase in land C sinks over the entire planet from 1995 to 2014, with the tropics accounting for around half of this increase in NEP despite being only around 22% of the global land (excluding Antarctica, **Table 2**). Therefore, preserving tropical ecosystems should be a global priority in order to mitigate anthropogenic CO_2 emissions. Temperature has diminished the capacity of terrestrial ecosystems to sequester C, which jeopardises future C sink capacity in light of global warming. So far, our results suggest that the benefit of increasing atmospheric concentrations of CO_2 are still compensating the negative ones of temperature rise, in terms of C sequestration. However, if it has not started to change already[6], this pattern may eventually reverse with saturation of land C sinks[5,31] or because warm ecosystems tend to decrease NEP as temperature rises (**Figure 2**). Additionally, the comparison between model results indicated that the DGVMs were unable to reproduce several features of the global land C sinks observed in inversion models. Process-based earth system models will need to improve their parameterisation to capture these features in order to better predict the future of land C sinks.

References:

1. Canadell, J. G. *et al.* Contributions to accelerating atmospheric CO2 growth from economic activity, carbon intensity, and efficiency of natural sinks. *Proc. Natl. Acad. Sci. U. S. A.* **104,** 18866–70 (2007).

2. Le Quéré, C. *et al.* Global Carbon Budget 2017. *Earth Syst. Sci. Data* **10,** 405–448 (2018).

3. Ciais, P. *et al.* Europe-wide reduction in primary productivity caused by the heat and drought in 2003. *Nature* **437,** 529–533 (2005).

4. Crowther, T. W. *et al.* Quantifying global soil carbon losses in response to warming. *Nature* **540,** 104–108 (2016).

5. Fernández-Martínez, M. *et al.* Atmospheric deposition, CO2, and change in the land carbon sink. *Sci. Rep.* **7:9632,** 1–13 (2017).

6. Peñuelas, J. *et al.* Shifting from a fertilization-dominated to a warming dominated period. *Nat. Ecol. Evol.* **1,** 1438–1445 (2017).

7. Ainsworth, E. A. & Long, S. P. What have we learned from 15 years of free-air CO2 enrichment (FACE)? A meta-analytic review of the responses of photosynthesis, canopy properties and plant production to rising CO2. *New Phytol.* **165,** 351–71 (2005).

8. Medlyn, B. E. *et al.* Using ecosystem experiments to improve vegetation models. *Nat. Clim. Chang.* **5,** 528–534 (2015).

9. Keenan, T. F. *et al.* Increase in forest water-use efficiency as atmospheric carbon dioxide concentrations rise. *Nature* **499,** 324–327 (2013).

10. Alexander, L. *et al.* *Climate Change 2013: The Physical Science Basis - Summary for Policymakers*. *Fifth Assessment Report* (Intergovernmental Panel on Climate Change, 2013).

11. Fernández-Martínez, M. *et al.* Spatial variability and controls over biomass stocks, carbon fluxes and resource-use efficiencies in forest ecosystems. *Trees, Struct. Funct.* **28,** 597–611 (2014).

12. Beer, C. *et al.* Terrestrial gross carbon dioxide uptake: global distribution and covariation with climate. *Science (80-.).* **329,** 834–8 (2010).

13. Luyssaert, S. *et al.* CO_2 balance of boreal, temperate, and tropical forests derived from a global database. *Glob. Chang. Biol.* **13,** 2509–2537 (2007).

14. de Vries, W. & Posch, M. Modelling the impact of nitrogen deposition, climate change and nutrient limitations on tree carbon sequestration in Europe for the period 1900–2050. *Environ. Pollut.* **159,** 2289–2299 (2011).

15. Wamelink, G. W. W. *et al.* Modelling impacts of changes in carbon dioxide concentration, climate and nitrogen deposition on carbon sequestration by European forests and forest soils. *For. Ecol. Manage.* **258,** 1794–1805 (2009).

16. Wamelink, G. W. W. *et al.* Effect of nitrogen deposition reduction on biodiversity and carbon sequestration. *For. Ecol. Manage.* **258,** 1774–1779 (2009).

17. de Vries, W., Du, E. & Butterbach-Bahl, K. Short and long-term impacts of nitrogen deposition on carbon sequestration by forest ecosystems. *Curr. Opin. Environ. Sustain.* **9–10,** 90–104 (2014).

18. Luyssaert, S. *et al.* The European carbon balance. Part 3: forests. *Glob. Chang. Biol.* **16,** 1429–1450 (2010).

19. Magnani, F. *et al.* The human footprint in the carbon cycle of temperate and boreal forests. *Nature* **447,** 848–50 (2007).

20. Thomas, R. B., Spal, S. E., Smith, K. R. & Nippert, J. B. Evidence of recovery of Juniperus virginiana trees from sulfur pollution after the Clean Air Act. *Proc. Natl. Acad. Sci. U. S. A.* **110,** 15319–24 (2013).

21. Oulehle, F. *et al.* Major changes in forest carbon and nitrogen cycling caused by declining sulphur deposition. *Glob. Chang. Biol.* **17,** 3115–3129 (2011).

22. Truog, E. Soil Reaction Influence on Availability of Plant Nutrients1. *Soil Sci. Soc. Am. J.* **11,** 305 (1946).

23. Fernández-Martínez, M. *et al.* Nutrient availability as the key regulator of global forest carbon balance. *Nat. Clim. Chang.* **4,** 471–476 (2014).

24. Zhu, Z. *et al.* Greening of the Earth and its drivers. *Nat. Clim. Chang.* **6,** 791–795 (2016).

25. Chevallier, F. *et al.* CO_2 surface fluxes at grid point scale estimated from a global 21 year reanalysis of atmospheric measurements. *J. Geophys. Res.* **115,**

D21307 (2010).

26. Rödenbeck, C., Houweling, S., Gloor, M. & Heimann, M. CO_2 flux history 1982–2001 inferred from atmospheric data using a global inversion of atmospheric transport. *Atmos. Chem. Phys.* **3,** 1919–1964 (2003).

27. Aber, J. *et al.* Forest Processes and Global Environmental Change: Predicting the Effects of Individual and Multiple Stressors. *Bioscience* **51,** 735 (2001).

28. Prentice, I. C., Heimann, M. & Sitch, S. The carbon balance of the terrestrial biosphere: Ecosystem models and Atmospheric observations. *Ecol. Appl.* **10,** 1553–1573 (2000).

29. Cheng, L. *et al.* Recent increases in terrestrial carbon uptake at little cost to the water cycle. *Nat. Commun.* **8,** 110 (2017).

30. Norby, R. J., Warren, J. M., Iversen, C. M., Medlyn, B. E. & McMurtrie, R. E. CO2 enhancement of forest productivity constrained by limited nitrogen availability. *Proc. Natl. Acad. Sci. U. S. A.* **107,** 19368–73 (2010).

31. Norby, R. J. *et al.* Forest response to elevated CO2 is conserved across a broad range of productivity. *Proc. Natl. Acad. Sci. U. S. A.* **102,** 18052–18056 (2005).

32. Van Groenigen, K. J. *et al.* The Impact of Elevated Atmospheric CO2 on Soil C and N Dynamics. *Ecol. Stud.* **187,** 374–391 (2006).

33. Terrer, C. *et al.* Mycorrhizal association as a primary control of the CO_2 fertilization effect. *Science* **353,** 72–4 (2016).

34. McCarthy, H. R. *et al.* Re-assessment of plant carbon dynamics at the Duke free-air CO2enrichment site: interactions of atmospheric [CO2] with nitrogen and water availability over stand development. *New Phytol.* **185,** 514–528 (2010).

35. Hyvönen, R. *et al.* The likely impact of elevated [CO2], nitrogen deposition, increased temperature and management on carbon sequestration in temperate and boreal forest ecosystems: a literature review. *New Phytol.* **173,** 463–80 (2007).

36. Ryan, M. G. Effects of climate change on plant respiration. *Ecol. Appl.* **1,** 157–167 (1991).

37. Amthor, J. S. Scaling CO2 Photosynthesis Relationships from the Leaf to the

Canopy. *Photosynth. Res.* **39,** 321–350 (1994).

38. Wu, Z., Dijkstra, P., Koch, G. W., Peñuelas, J. & Hungate, B. a. Responses of terrestrial ecosystems to temperature and precipitation change: a meta-analysis of experimental manipulation. *Glob. Chang. Biol.* **17,** 927–942 (2011).

39. Chevallier, F. *et al.* Toward robust and consistent regional CO2 flux estimates from in situ and spaceborne measurements of atmospheric CO2. *Geophys. Res. Lett.* **41,** 1065–1070 (2014).

40. Olivier, J. G. J. & Berdowski, J. J. M. in *The Climate System* (eds. Berdowski, J., Guicherit, R. & Heij, B. J.) 33–78 (2001).

41. Sitch, S. *et al.* Recent trends and drivers of regional sources and sinks of carbon dioxide. *Biogeosciences* **12,** 653–679 (2015).

42. Harris, I., Jones, P. D. D., Osborn, T. J. J. & Lister, D. H. H. Updated high-resolution grids of monthly climatic observations - the CRU TS3.10 Dataset. *Int. J. Climatol.* **34,** online, update (2013).

43. Vicente-serrano, S. M., Beguería, S. & López-Moreno, J. I. A Multiscalar Drought Index Sensitive to Global Warming: The Standardized Precipitation Evapotranspiration Index. *J. Clim.* **23,** 1696–1718 (2010).

44. Zuur, A., Ieno, E., Walker, N., Saveliev, A. & Smith, G. *Mixed effects models and extensions in ecology with R*. (Springer science, 2009).

45. Mathias, J. M. & Thomas, R. B. Disentangling the effects of acidic air pollution, atmospheric CO2, and climate change on recent growth of red spruce trees in the Central Appalachian Mountains. *Glob. Chang. Biol.* **24,** 3938–3953 (2018).

46. R Core Team. R: A Lenguage and Environment for Stasitical Computing. (2016).

47. Barton, K. MuMIn: Multi-model inference. R package version 1.17.1. http://CRAN.R-project.org/package=MuMIn. (2015).

48. Nakagawa, S. & Schielzeth, H. A general and simple method for obtaining R 2 from generalized linear mixed-effects models. *Methods Ecol. Evol.* **4,** 133–142 (2013).

49. Breheny, P. & Burchett, W. Visualization of Regression Models Using visreg, R package version 2.2-0. (2015).

Correspondence and requests for materials should be addressed to:

Marcos Fernández-Martínez: marcos.fernandez-martinez@uantwerpen.be

Acknowledgements

This research was supported by the Spanish Government project CGL2016-79835-P (FERTWARM), the European Research Council Synergy grant ERC-2013-726 SyG-610028 IMBALANCE-P, and the Catalan Government project SGR 2017-1005. M.F-M and S.V. are a postdoctoral fellows of the Research Foundation – Flanders (FWO). J.G.C. thanks the support of the National Environmental Science Programme ESCC Hub. We thank Christian Röedenbeck for his advice and for distributing Jena CarboScope and all the modellers that contributed to the TRENDY project.

Author Contributions

M.F-M., J.S., I.A.J., and J.P. conceived, analyzed and wrote the paper. F.C., P.F., and S.S., provided data. All authors contributed substantially to the writing and discussion of the paper.

Figure captions

Figure 1: Global trends in NEP and their contributing factors. Global temporal contributions of CO_2, climate and land-use change to the trends in NEP (annual change) are shown on the right side of each panel. The difference between the modelled temporal contributions and the trends (shaded) has been treated as an unknown contribution to the temporal variation in NEP. Statistically significant (P < 0.01) temporal variations of the predictors are shown in square brackets. Error bars indicate 95% confidence intervals. The boxplots in panel c indicate the estimated contributions of the 10 DVGMs used in the TRENDY ensemble. Units are ppm y^{-1} for CO_2, °C y^{-1} for temperature, mm y^{-2} for precipitation, standard deviation for SPEI, and percentage of land-use cover per pixel for forests, crops, and urban areas. See the Materials and Methods section for information about the methodology used to calculate the contributions. Significance levels: *, $P < 0.01$; **, $P < 0.005$; ***, $P < 0.001$.

Figure 2: Plots showing the estimated effects of the interactions of the statistical models. The graphs show interactions between CO_2 and climate (mean annual precipitation [MAP] and temperature [MAT], and annual anomalies in temperature [MAT.an]) on NEP for the MACC-II and Jena CarboScope inversion models and the TRENDY ensemble. Shaded bands indicate the 95% confidence intervals of the slopes. Non-significant interactions are indicated by "n.s.".

Table 1: Global and latitudinal analyses of sensitivity of NEP to changes in atmospheric CO_2 concentrations and mean annual temperature. The "%" columns indicate the contribution of the latitudinal band to the global estimate. Differences are calculated as the difference between the sum of all latitudinal bands and the global estimate. Bold coefficients differ significantly from 0 at the 0.01 level. Empty cells indicate that anomalies in temperature were not a significant predictor in the models predicting NEP. Units are Tg C y^{-1} ppm^{-1} for CO_2 and Tg C y^{-1} C^{-1} for temperature.

Table 2: Global and latitudinal trends and temporal contributions of changes in atmospheric CO_2 concentrations and mean annual temperature to NEP trends. The "%" columns indicate the percentage of contribution of each latitudinal band to the global estimate. Columns "Cont." show the percentage of contribution of CO_2 and temperature to the trends in NEP. Column "Other" shows the difference between the NEP trend and the sum of contributions of CO_2 and temperature. If different from zero, it indicates that other factors are contributing to the trends in NEP. The "differences" rows are calculated as the difference between the sum of all latitudinal bands and the

global estimate. NH and SH indicate Northern and Southern Hemispheres, respectively. Bold coefficients differ significantly from 0 at the 0.01 level. Empty cells indicate that anomalies in temperature were not a significant predictor in the models predicting NEP. Units are Tg C y^{-1} for trends, Tg C y^{-1} ppm^{-1} for CO_2 and Tg C y^{-1} C^{-1} for temperature. Errors were calculated using the error propagation method. See the Materials and Methods section for information about the methods used to calculate the contributions.

Figure 1

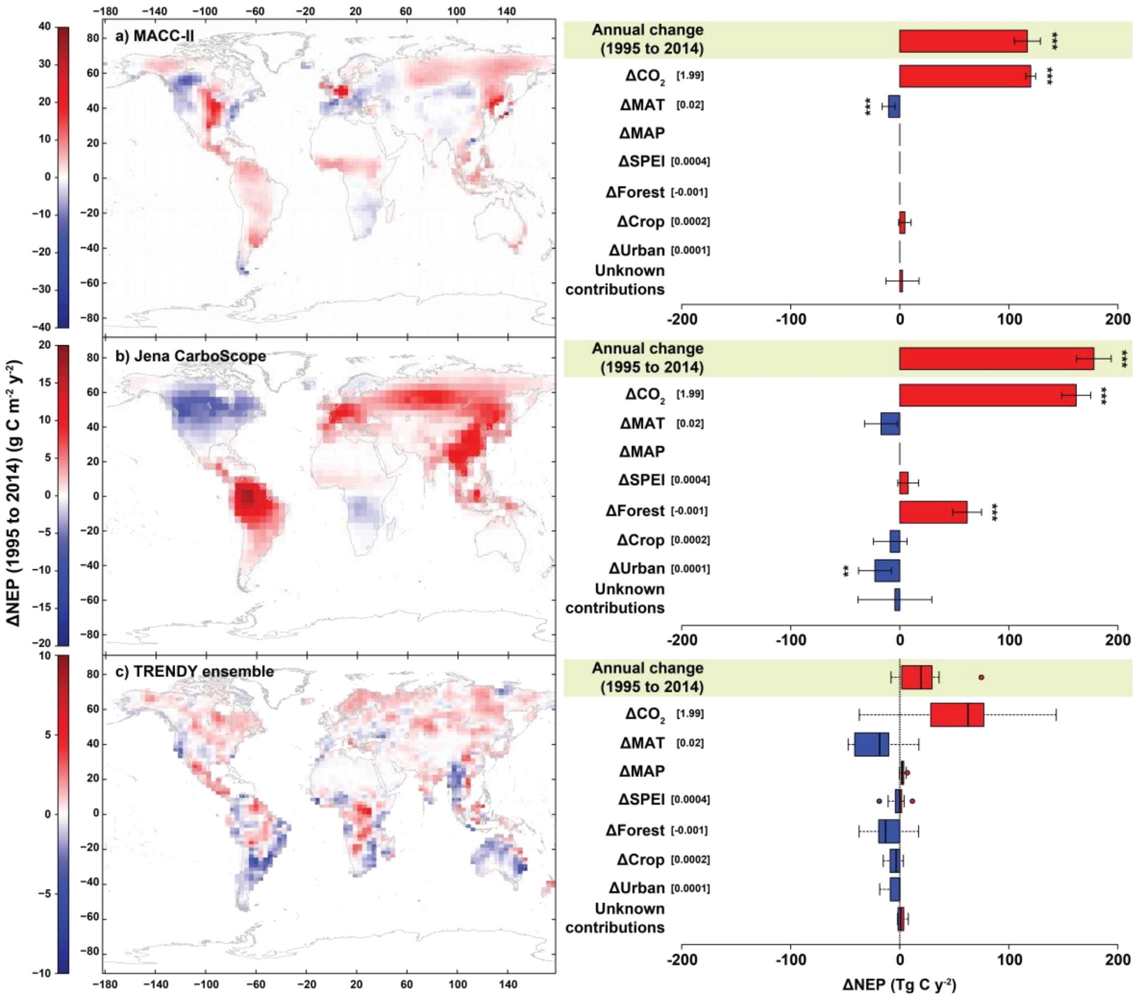

a) MACC-II
b) Jena CarboScope
c) TRENDY ensemble
ΔNEP (1995 to 2014) (g C m-2 y-2)
Annual change
(1995 to 2014)
ΔCO2 [1.99]
ΔMAT [0.02]
ΔMAP
ΔSPEI [0.0004]
ΔForest [-0.001]
ΔCrop [0.0002]
ΔUrban [0.0001]
Unknown
contributions
ΔNEP (Tg C y-2)

Figure 2

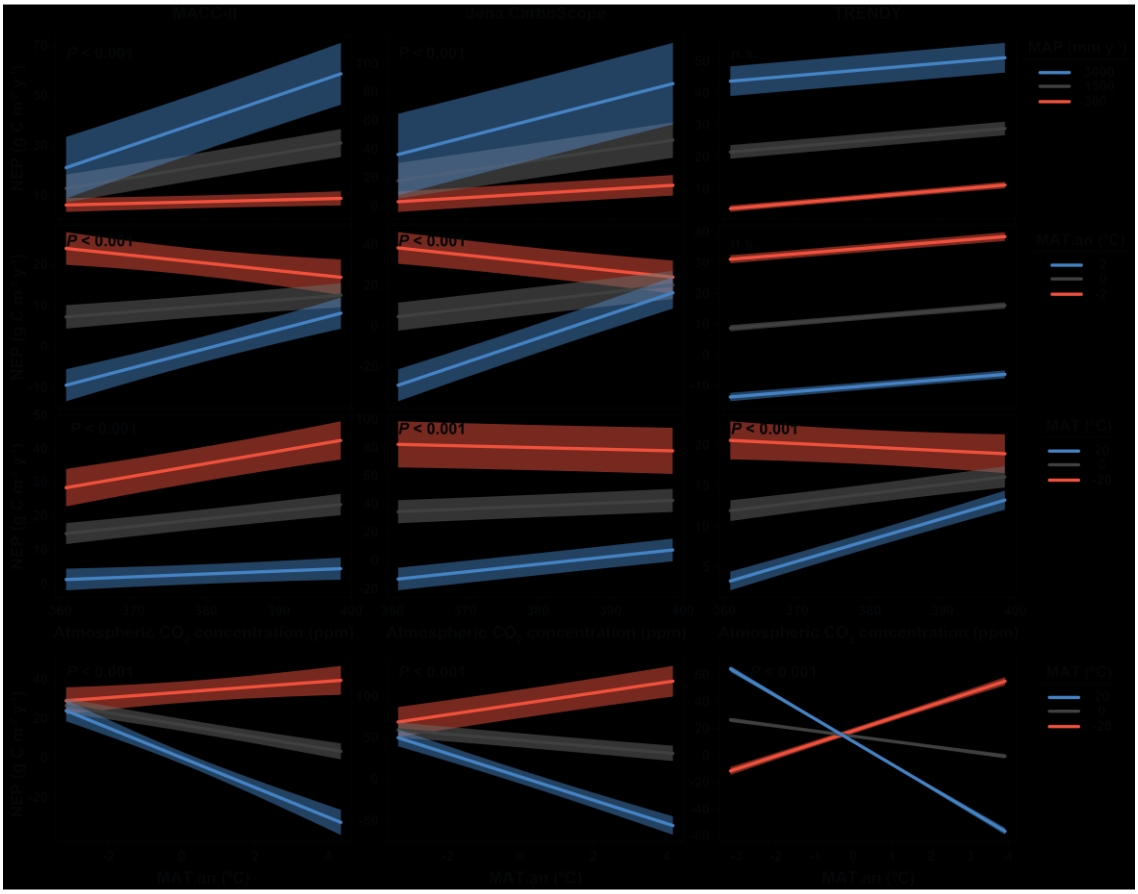

Table 1

	CO_2	%	Temperature	%
MACC				
NH >55°	**8.5 ± 0.4**	14.1	-35.3 ± 24.1	6.8
NH 35-55°	**14.7 ± 1.3**	24.3	-132.0 ± 259.9	25.6
NH 15-35°	**-5.0 ± 1.4**	-8.3		
NH 15-SH 15°	**31.9 ± 0.7**	52.9	101.9 ± 216.6	-19.8
SH 15-35°	**2.2 ± 0.9**	3.7	-150.2 ± 131.3	29.1
SH 35-55°	0.6 ± 0.3	1.0	-13.4 ± 49.3	2.6
Global	**60.4 ± 1.2**		**-515.7 ± 152.4**	
Difference	**-7.4 ± 2.6**	-12.3	286.6 ± 397.4	-55.6
JENA				
NH >55°	-0.3 ± 1.0	-0.3	-49.8 ± 48.2	5.8
NH 35-55°	**11.1 ± 3.9**	13.6	-213.6 ± 558.1	24.9
NH 15-35°	**26.3 ± 2.7**	32.3	-268.7 ± 400.0	31.3
NH 15-SH 15°	**54.2 ± 3.6**	66.6	-697.6 ± 1136.5	81.2
SH 15-35°	**5.4 ± 0.9**	6.6	-167.0 ± 133.9	19.4
SH 35-55°	**0.2 ± 0.0**	0.3		
Global	**81.4 ± 3.4**		-859.2 ± 386.3	
Difference	15.4 ± 6.9	19.0	-537.4 ± 1390.2	62.5
TRENDY				
NH >55°	**2.8 ± 0.1**	9.0	**17.3 ± 7.3**	-1.6
NH 35-55°	**5.8 ± 0.5**	19.0	**-251.1 ± 79.3**	23.1
NH 15-35°	**5.9 ± 0.6**	19.4	**-368.8 ± 51.9**	33.9
NH 15-SH 15°	**16.6 ± 1.1**	54.2	**-1612.2 ± 213.4**	148.2
SH 15-35°	**4.6 ± 1.2**	14.9	**-379.2 ± 141.1**	34.9
SH 35-55°	0.3 ± 0.2	1.0	-36.8 ± 18.1	3.4
Global	**30.7 ± 1.2**		**-1088.0 ± 118.1**	
Difference	**5.4 ± 2.1**	17.5	**-1542.7 ± 298.0**	141.8

Table 2

	Trends	**%**	**CO_2**	**%**	**Cont.**	**Temp**	%	**Cont.**	**Other**
MACC									
NH >55°	**20.1 ± 1.2**	17.2	**17.0 ± 0.8**	14.1	84.4	-1.2 ± 0.8	11.5	-5.9	4.3 ± 1.7
NH 35-55°	**17.5 ± 5.0**	15.0	**29.2 ± 2.7**	24.3	166.6	-1.7 ± 3.2	16.1	-9.4	-10.0 ± 6.5
NH 15-35°	**14.0 ± 3.1**	12.0	-9.9 ± 2.8	-8.3	-71.0			0.0	**23.9 ± 4.1**
NH 15-SH 15°	**55.4 ± 2.7**	47.4	**63.5 ± 1.5**	52.9	114.6	0.9 ± 1.9	-8.9	1.6	-9.0 ± 3.6
SH 15-35°	**7.6 ± 1.4**	6.5	**4.4 ± 1.9**	3.7	57.6	-2.3 ± 2.0	22.2	-29.8	5.5 ± 3.1
SH 35-55°	**2.3 ± 0.6**	2.0	1.2 ± 0.7	1.0	49.9	-0.3 ± 1.0	2.5	-11.2	1.4 ± 1.3
Global	**116.9 ± 6.1**		**120.1 ± 2.3**		102.7	**-10.3 ± 3.0**		-8.8	7.1 ± 7.2
Difference	0.0 ± 9.1	0.0	**-14.8 ± 5.2**	-12.3		5.8 ± 5.4	-56.6		
JENA									
NH >55°	**13.8 ± 2.2**	7.7	-0.5 ± 2.1	-0.3	-3.8	-1.7 ± 1.7	9.9	-12.4	**16.0 ± 3.5**
NH 35-55°	**49.8 ± 5.9**	28.0	**22.0 ± 7.7**	13.6	44.1	-2.7 ± 6.9	15.4	-5.3	**30.5 ± 11.9**
NH 15-35°	**49.2 ± 4.0**	27.6	**52.3 ± 5.3**	32.3	106.2	-5.0 ± 7.4	29.0	-10.2	1.9 ± 10.0
NH 15-SH 15°	**80.4 ± 5.1**	45.2	**107.7 ± 7.1**	66.6	133.9	-5.7 ± 9.2	32.9	-7.0	-21.6 ± 12.7
SH 15-35°	**10.4 ± 1.3**	5.8	**10.7 ± 1.7**	6.6	103.1	-2.8 ± 2.2	16.2	-26.9	2.5 ± 3.1
SH 35-55°	**0.5 ± 0.1**	0.3	**0.4 ± 0.1**	0.3	87.2				0.1 ± 0.1
Global	**178.0 ± 8.1**		**161.8 ± 6.8**		90.9	**-17.2 ± 7.7**		-9.7	**33.4 ± 13.1**
Difference	**26.1 ± 12.2**	14.7	**30.7 ± 13.8**	19.0		-0.6 ± 16.0	3.4		
TRENDY									
NH >55°	**9.3 ± 0.6**	41.4	**5.5 ± 0.3**	9.0	59.0	**0.6 ± 0.2**	-2.7	6.1	**3.3 ± 0.7**
NH 35-55°	**9.4 ± 1.3**	41.5	**11.6 ± 0.9**	19.0	124.0	**-3.0 ± 0.9**	13.9	-31.6	0.7 ± 1.8
NH 15-35°	**3.3 ± 1.3**	14.9	**11.8 ± 1.1**	19.4	352.9	**-7.9 ± 1.0**	36.9	-235.0	-0.6 ± 2.0
NH 15-SH 15°	**10.1 ± 2.3**	45.0	**33.0 ± 2.1**	54.2	326.2	**-17.2 ± 1.8**	80.8	-170.2	-5.7 ± 3.6
SH 15-35°	**-13.7 ± 1.8**	-60.9	**0.5 ± 0.1**	0.9	-3.8	**-0.3 ± 0.1**	1.6	2.5	**-13.9 ± 1.8**
SH 35-55°	**-1.0 ± 0.4**	-4.7	**0.6 ± 0.5**	1.0	-55.4	-0.7 ± 0.4	3.5	70.4	-0.9 ± 0.7
Global	**22.5 ± 3.1**		**61.0 ± 2.5**		270.7	**-21.3 ± 2.2**		-94.7	**-17.1 ± 4.5**
Difference	-5.2 ± 4.7	-22.9	2.1 ± 3.6	3.4		**-7.3 ± 3.2**	34.0		

Methods

Datasets

NEP data

We used gridded global monthly NEP data for 1995–2014 from two inversion models: i) the MACC (Monitoring Atmospheric Composition and Climate) CO_2 (http://www.gmes-atmosphere.eu/catalogue/) [25,39] database, version v14r2 and ii) the Jena CarboScope database version s93_v3.7 using a constant network of towers (http://www.bgc-jena.mpg.de/CarboScope/) [26]. The MACC CO_2 atmospheric inversion system relies on the variational formulation of Bayes' theorem to analyse direct measurements of CO_2 concentrations from 130 sites around the globe for 1979-2014. Optimised fluxes were calculated at a global horizontal resolution of 3.75 × 1.875° (longitude, latitude) and a temporal resolution of eight days, separately for daytime and night-time. The underlying transport model was run with interannually varying meteorological data from the ECMWF ERA-Interim reanalysis. The Jena inversion model estimates the interannual variability of CO_2 fluxes based on raw CO_2 concentration data from 50 sites. The model uses a variational approach with the TM3 transport model (4 × 5°, using interannually varying winds). Prior terrestrial fluxes were obtained from a modelled mean biospheric pattern and fossil-fuel emissions from the EDGAR emission database[40]. We also used NEP data from an ensemble of 10 dynamic global vegetation models (DGVMs) compiled by the TRENDY project (version 4, models CLM4.5, ISAM, JSBACH, JULES, LPJG, LPX, OCN, ORCHIDEE, VEGAS, and VISIT) to see if results obtained from atmospheric inversions data match those obtained with DGVMs simulations[41]. We used the output from simulation experiment S3, which was run with varying atmospheric CO_2 and changing land use and climate[41].

Meteorological, land-use change and atmospheric CO_2 data

We extracted gridded temperature and precipitation time series from the Climatic Research Unit TS3.23 dataset [42]. We also used the SPEI (Standardised Precipitation-Evapotranspiration Index) drought index[43] from the global SPEI database (http://SPEI.csic.es/database.html) as a measure of drought intensity (positive values indicate wetter than average meteorological conditions, negative values indicate drier than average conditions). We used annual SPEI1 (monthly SPEI averaged over a year). Mean annual temperature (MAT) and precipitation (MAP) and SPEI were calculated for each year and pixel. We used land-use change maps from land-use harmonisation[2] (LUH2, http://luh.umd.edu/data.shtml) and calculated the percent coverages of forests, croplands, and urban areas per pixel, so we could further estimate whether they increased or decreased from 1995 to 2014. We used the data for atmospheric CO_2 concentration from Mauna Loa Observatory provided by the Scripps Institution of Oceanography (Scripps CO_2 programme).

Data for N and S deposition

Annual data for N (oxidised N [N_{OX}] from NO_3^- and reduced N [N_{RED}] from NH_4^+) and S (SO_4^-) wet deposition were extracted from: i) the European Monitoring and Evaluation Programme (EMEP) with a spatial resolution of 0.15 × 0.15° for longitude and latitude, ii) the MSC-W chemical-transport model developed to estimate regional atmospheric dispersion and deposition of acidifying and eutrophying N and S compounds over Europe, and iii) the National Atmospheric Deposition Program (NADP) covering the USA with a spatial resolution of 0.027 × 0.027° for longitude and latitude. We used only data for wet deposition because the NADP database only contained records for dry deposition for 2000. Analyses focused on atmospheric deposition and were restricted to Europe and the USA because temporal gridded maps of atmospheric deposition were not available for other regions. Maps of atmospheric deposition for the regional analyses were adjusted to the resolution of the C-flux maps (3.75 × 1.875° for the MACC-II model and 4 × 5° for the Jena CarboScope model for longitude and latitude).

Statistical analyses

Gridded, global and regional trend detection on NEP

To determine how NEP has changed from 1995 to 2014, we first calculated the trends for each pixel in both inversion models and an average dataset of the TRENDY ensemble using linear regressions with an autoregressive and moving-average (ARMA) (autoregressive structure at lag p=1, and no moving average q=0) correlation structure to account for temporal autocorrelation. Trends over larger areas (e.g. the entire world, latitudinal bands), either for NEP or the predictor variables, were calculated using generalised linear mixed models (GLMMs) with random slopes, including also random intercepts[44] (e.g. NEP ~ year). We used pixel as the random factor (affecting the intercepts and slopes of the year), and an ARMA (p=1, q=0) correlation structure. All average trends shown were calculated using this methodology.

Calculation of temporal contributions on trends of NEP

The temporal contributions of increasing CO_2, climate (MAT, MAP, and SPEI), and land-use change (forests, croplands, and urban areas) to the observed trends in NEP were assessed for the MACC-II, Jena CarboScope, and TRENDY datasets for the entire world. We repeated the analysis for five latitudinal bands to determine if the contributions of CO_2, climate, and land-use change were globally consistent using MACC-II, Jena CarboScope, and the mean ensemble of the TRENDY datasets. For the MACC-II and Jena CarboScope datasets, we also determined the temporal contribution of atmospheric deposition of N (N_{OX} and N_{RED}) and S to the trends in NEP in a combined analysis that also included CO_2, climatic, and land-use trends. This latter analysis was restricted to Europe and the USA due to the lack of atmospheric-deposition time series for the rest of the world.

The temporal contributions of the predictor variables were calculated following the methodology established in references[5,45], as follows:

i) using a GLMM with an autocorrelation structure for lag 1 (AR1) and using the pixel as the random factor affecting only the intercept, we fitted full models for NEP as a function of CO_2, mean MAT per pixel, annual anomaly of MAT, mean MAP per pixel, annual anomaly of MAP, the annual SPEI, and mean percentage of forested, cropped, and urban areas per pixel and their annual anomalies. We included the first-order interaction terms between CO_2 and all predictors and between the mean values and the anomalies for all predictors (except SPEI, which interacted with mean MAT and MAP). When the interaction term between the means and the anomalies (e.g. MAT mean × MAT anomaly) was included, the model estimated the effect of the anomaly as a function of the average value. This implies a change in the effect of increasing or decreasing the anomalies, depending on the mean for the site (e.g. increasing temperature may have a positive effect in cold climates but a negative effect in warmer climates). For models including atmospheric deposition, we also included the interaction between climatic variables and CO_2 and the interactions between the means and the annual anomalies of atmospheric deposition (N_{OX}, N_{RED}, and S). The models were fitted using maximum likelihood to allow the comparison of models with different fixed factors.

ii) We used the stepwise backwards-forwards model selection (*stepAIC* function in R[46]) from the full models, using the lowest Bayesian information criterion (BIC), to obtain the best model. The amount of the variance explained by the models was assessed using the *r.squaredGLMM* function in R (MuMIn package: [47]) following the method of Nakagawa and Schielzeth (2013). Model residuals met the assumptions required in all analyses (normality and homoscedasticity of residuals).

iii) We then used the selected models to predict the changes of the response variables during the study period (1995–2014). We first extracted the observed trend (mean ± SEM, standard error of the mean) in NEP using raw data with GLMMs with an AR1 autocorrelation structure. We then calculated the trend of NEP predicted by the final model and the trends of NEP predicted by the same model while maintaining the temporally varying predictors (i.e., anomalies) constant one at a time (e.g. MAT anomalies were held constant using the median per pixel, while all other predictors changed based on the observations). The difference between the predictions for the final model and when one predictor was controlled was assumed to be the contribution of that predictor variable to the change in NEP. The differences between all individual contributions and the observed trend in NEP were treated as unknown contributions.

Calculation of sensitivities of NEP to temporal predictors

Finally, we calculated the average sensitivities of NEP to the predictor changes by dividing the temporal contributions of each predictor of delta NEP by their temporal trends. Spatial variability on the effects of temporal predictors to NEP were assessed using the GLMMs fitted to estimate the temporal contributions of the predictors. To visualise the interactions we used the R package visreg[49]. All errors were calculated using the error-propagation method using the following two equations, for additions and subtractions: $\boldsymbol{\varepsilon C} = \sqrt{(\boldsymbol{\varepsilon A})^2 + (\boldsymbol{\varepsilon B})^2}$; and for multiplications and divisions: $\boldsymbol{\varepsilon C} = \boldsymbol{C}\sqrt{\left(\frac{\boldsymbol{\varepsilon A}}{\boldsymbol{A}}\right)^2 + \left(\frac{\boldsymbol{\varepsilon B}}{\boldsymbol{B}}\right)^2}$; where ε indicates the error associated to each value (A, B or C). To calculate global and regional estimates we multiplied the model outputs, in units of gC m^{-2}, times land area. We considered the land Earth surface area to be 134375000 km^2 excluding the Antarctic region. Land area for the different latitudinal bands used were: >55º N, 23818000 km^2; 35 to 55º N, 31765000 km^2; 15 to 35º N, 29213000 km^2; 15º S to 15º N, 29926000 km^2; 15 to 35º S, 17308000 km^2; and 35 to 55º S, 2345600 km^2.

Data availability

The authors declare that the data supporting the findings of this study are publically available in the webpages provided in the article. The TRENDY simulations are available from the corresponding author upon request.